Clinical Anatomy 00:00–00 (2015)

ORIGINAL COMMUNICATION

External Rib Structure Can Be Predicted Using Mathematical Models:
An Anatomical Study With Application to Understanding Fractures and Intercostal Muscle Function

AARON R CASHA,[1,2]* LIBERATO CAMILLERI,[3] ALEXANDER MANCHÉ,[2] RUBEN GATT,[4] DAPHNE ATTARD,[4] MARILYN GAUCI,[5] MARIE-THERESE CAMILLERI-PODESTA,[2] AND JOSEPH N. GRIMA[4]

[1]*Department of Anatomy, University of Malta, Msida, Malta*
[2]*Department of Cardiothoracic Surgery, Mater Dei Hospital, Msida, Malta*
[3]*Department of Statistics and Operations Research, Faculty of Science, University of Malta, Malta*
[4]*Metamaterials Unit, Faculty of Science, University of Malta, Msida, Malta*
[5]*Department of Anaesthesia, Mater Dei Hospital, Msida, Malta*

As ribs adapt to stress like all bones, and the chest behaves as a pressure vessel, the effect of stress on the ribs can be determined by measuring rib height and thickness. Rib height and thickness (depth) were measured using CT scans of seven rib cages from anonymized cadavers. A Finite Element Analysis (FEA) model of a rib cage was constructed using a validated approach and used to calculate intramuscular forces as the vectors of both circumferential and axial chest wall forces at right angles to the ribs. Nonlinear quadratic models were used to relate rib height and rib thickness to rib level, and intercostal muscle force to vector stress. Intercostal muscle force was also related to vector stress using Pearson correlation. For comparison, rib height and thickness were measured on CT scans of children. Rib height increased with rib level, increasing by 13% between the 3rd and 7th rib levels, where the 7th/8th rib was the widest part or "equator" of the rib cage, $P < 0.001$ (t-test). Rib thickness showed a statistically significant 23% increase between the 3rd and 7th ribs, $P = 0.004$ (t-test). Intercostal muscle force was significantly related to vector stress, Pearson correlation $r = 0.944$, $P = 0.005$. The three nonlinear quadratic models developed all had statistically significant parameter estimates with $P < 0.03$. External rib morphology, in particular rib height and thickness, can be predicted using statistical mathematical models. Rib height is significantly related to the calculated intercostal muscle force, showing that environmental factors affect external rib morphology. Clin. Anat. 00:000–000, 2015.

Key words: rib; biomechanics; morphology; anatomy; Laplace law; pressure vessel

INTRODUCTION

Ribs are long curved bones that form the rib cage in vertebrates (Kurihara, 1999). In most vertebrates they surround the chest only (Britz and Bartsch, 2003) and facilitate breathing by providing a rigid cavity that enables the lungs to expand. They also serve to protect the heart, the lungs, and to some extent other internal

*Correspondence to: Dr Aaron Casha, Department of Cardiothoracic Surgery, Mater Dei Hospital, Msida MSD 2090, Malta. E-mail: aaron.casha@um.edu.mt

Received 10 June 2014; Revised 26 December 2014; Accepted 6 January 2015

Published online in Wiley Online Library (wileyonlinelibrary.com). DOI: 10.1002/ca.22513

organs such as the liver. In snakes and some other animal groups, ribs are used to provide support, some forms of locomotion and protection for the whole body (Astley and Jane, 2007).

Since ribs in mammals usually cover only the thoracic cavity, they are exposed to the changing forces and pressures within the thorax during breathing and coughing. During coughing, the thoracic cavity acts as a biological pressure vessel or hollow organ with contents at a distending pressure (Casha, 2012) and the ribs act as strengthening structures or filaments within its wall. Breathing results in loads similar to coughing, but lower in magnitude and much more frequent, comparable to an open pressure vessel (Papadakis, 1977).

According to Wolff's law, skeletal structures adapt to support their musculoskeletal loads. Bones remodel their architecture so that they can withstand these loads (Beck, 2001). In Harold Frost's Mechanostat model, bone growth is stimulated by local peak mechanical elastic bone deformation (Frost, 2003). For ribs, the peak load is caused by the forces induced by coughing (Murray, 1994). The resultant vector of the forces induced by coughing and breathing also acts on the ribs, inducing them to align with its direction. The force acting on the ribs results in a change in rib morphology as an adaptation to the load.

Although Pascal's principle states that the pressure of a gas is the same everywhere inside a pressure vessel at equilibrium (Halliday, 1997), there are significant differences in wall tension among different parts of such a vessel. The relationship between wall tension and pressure vessel dimensions is described by Laplace's law: the formula involved depends on vessel wall shape (Pender, 2009), but wall tension is proportional to the effective radius at the tangent to the curvature (Young, 2002). The direction and magnitude of chest wall forces vary with chest wall shape and location within the chest.

The chest wall has been modeled as a pressure vessel to obtain measurements of the rib forces at the mid-axillary line using a validated model (Casha, 2014) (Fig. 1). Pressure vessel modeling predicted that rib height would be stretched in direct proportion to the resultant intercostal muscular force at 90° to the ribs, from the fetal starting-point of nearly identical round ribs, resulting in tall ribs near the equator of the ellipsoid gradually diminishing in tangential height towards the apex, explaining the differences in postnatal rib growth with rib level (Grivas, 1992). The thickness and height of each rib were measured using three-dimensional software. In another part of the study, theoretical values of the intercostal intramuscular stresses acting on the ribs were calculated from finite element analysis (FEA) simulation. Measured rib heights were then related to those theoretical values in order to assess how the Wolff's law relationship affects the ribs. This could elucidate the variations of stress over the chest wall, with potentially important implications for chest wall reconstruction.

METHODS

External Bone Dimensions

A series of high resolution CT scans, using fine section CT cuts of seven rib cages from anonymized cadavers in a dissection room, were resliced, reconstructed and analyzed using Osirix DICOM viewing software (Pixmeo, Switzerland) with the following settings: pulmonary window level and window width (WL/WW), UCLA color look-up table (CLUT), coronal orientation and maximum intensity projection (MIP) with thin level slices. Rib height and rib thickness (depth) were measured at right angles to the long axis of the ribs in the mid-axillary line (Fig. 2) and localized using three simultaneous views in three adjustable planes. Cadaveric material was used so that high CT scan tube voltages could be deployed, with the maximal number of cuts and overlaps between cuts, maximizing the CT scanner's spatial resolution.

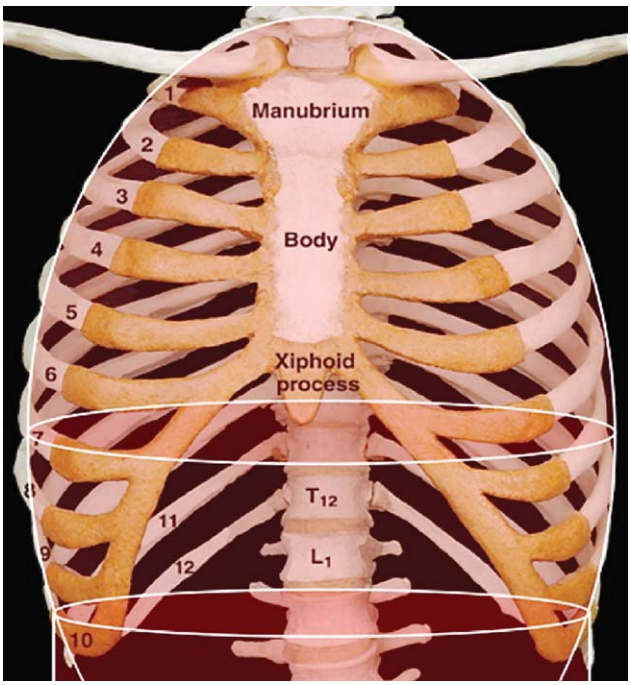

Fig. 1. Model of rib cage with an ellipsoid and cylindrical waist section. [Color figure can be viewed in the online issue, which is available at wileyonlinelibrary.com.]

Calculation of Intramuscular Forces

Intramuscular forces were calculated as the vectors of both circumferential and axial chest wall forces at right angles to the ribs at the mid-axillary line using a thin-wall FEA ellipsoid pressure vessel model with 12 cm coronal radius, 11 cm sagittal radius and 21 cm vertical height, following established procedures (Casha, 2014). The model assumed isotropy, with the chest wall modeled as a homogenous elastic material with properties chosen to correspond to the upper-bound limit defined by the rule of mixtures for a composite of matrix and fiber:

$$E_c = E_m V_m + E_f V_f$$

Where E_i is the elastic modulus, V_i is the volume fraction, m represents the muscular matrix, and f

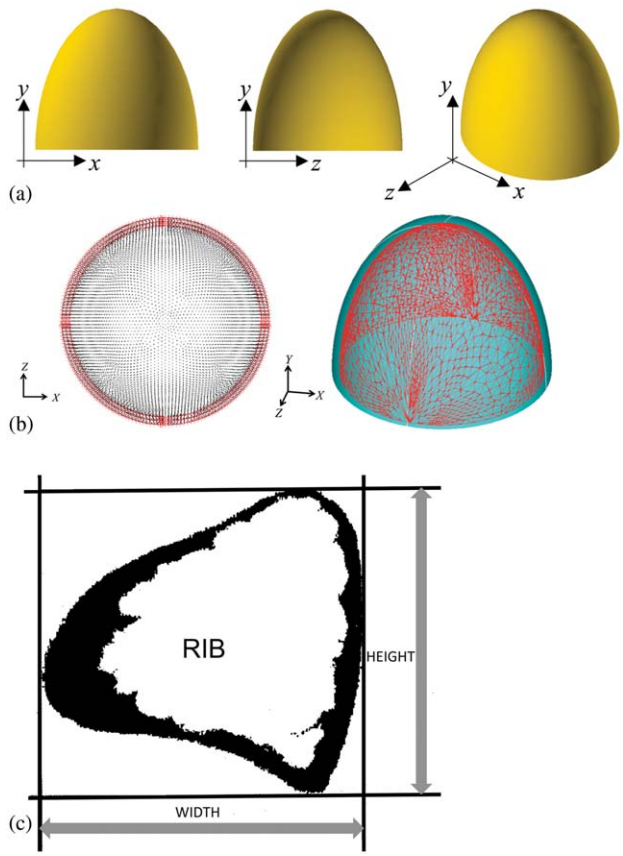

Fig. 2. (**a**) Views and (**b**) boundary and loading conditions for the ellipsoid FEA chest model. (**c**) Diagram showing measurements performed on the ribs. Height was measured tangential to the plane of the curvature of the ribs in the mid-axillary line. [Color figure can be viewed in the online issue, which is available at wiley onlinelibrary.com.]

represents the rib acting as a fiber. This formula yields the highest Young's modulus possible in this scenario. The Young's modulus for bones in the ribs was taken as 7 GPa, which is representative of an adult population (Pezowicz and Glowacki, 2012), while the Young's modulus for muscle was taken as 1.5 kPa {Chen, 1996). The volume fractions were assumed to be 50% bone and 50% muscle, giving a Young's modulus of 3.5 GPa for the chest wall. This Young's modulus, and the 0.3 value for Poisson's ratio (Li, 2010), were used as parameters in the finite element analysis (FEA) model. This model was then meshed using SOLID187 element, a 3D ten-node tetrahedral structural solid element with three degrees of freedom at each node, i.e., translation in the nodal *x*-, *y*-, and *z*- directions. The nodes at the bottom-most part of the chest wall were fixed in the *y*-direction. The center-lines parallel to the *x*-axis at the bottom edge were fixed in the *z*-direction, while those parallel to the *z*-direction were fixed in the *x*-direction (Fig. 2). Ansys® (Ansys Inc., Canonsburg, USA) was used for FEA simulations with scripting in ADPL (ANSYS Parametric Design Language). The ellipsoid shell model was constrained at its base and subjected to a 40 kPa internal distending pressure (Lumb, 2000).

Rib Dimensions With Development

The ribs in a mounted fetal skeleton, two children and two adolescents were measured using Osirix DICOM software at right angles to their long axes. Thoracic CT scans were chosen on a random basis, any thoracic pathology having been excluded.

Local ethics committee approval was obtained for this study.

Assumptions

Various assumptions were made to simplify the model:

1. the chest wall forces are transmitted through bones only;
2. the weight of the head, neck and arms passes through the spinal column and has no effect on chest wall biomechanics;
3. the shape of the chest wall is simplified to a scalene ellipsoid, i.e. with an oval transverse section and an ellipsoid apex. This model is inaccurate at the level of the back since the human spinal column is located deeply within the trunk to improve the centre of gravity with an upright posture;
4. force vectors parallel to the rib from the external and internal intercostal muscles cancel each other (assuming equal external and internal intercostal muscle masses), while the vector forces at 90° to the rib are summed together. In reality, this holds at the mid-axillary line but not at the level of the internal and external intercostal membranes.

Statistics

SPSS (IBM Inc., Armonk, USA) was used to fit a nonlinear quadratic model relating rib height to rib

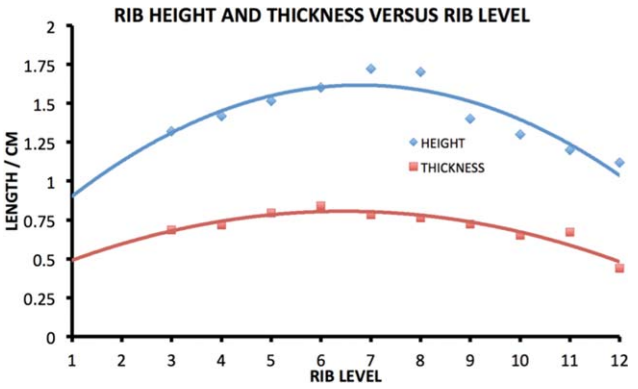

Fig. 3. Graph showing rib height and thickness against rib level. Note that both rib height and thickness are related to the radius of the chest at their level. The maximum ("equator") occurs between the 6th and 7th ribs. [Color figure can be viewed in the online issue, which is available at wileyonlinelibrary.com.]

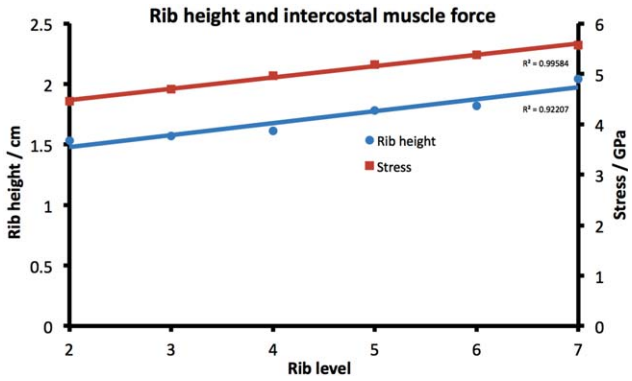

Fig. 4. Graph displaying the linear relationships of rib height and estimated intercostal muscle force to rib level. It also shows how the intercostal muscle acts to stretch rib height, with intercostal muscle force varying according to the ellipsoid pressure vessel model. [Color figure can be viewed in the online issue, which is available at wileyonlinelibrary.com.]

level. Similarly, a quadratic model was used to relate rib thickness to rib level. General quadratic equations are of the form:

$$y = ax^2 + bx + c$$

where y is the predicted rib parameter and x is the rib level. The parameters *a, b*, and *c* were estimated using maximum likelihood estimation, and goodness of fit was assessed using the *R*-square value. The tables below display the parameter estimates with standard errors and 95% confidence intervals, while the overlay scatter plots relate the measured rib heights and thicknesses, and those estimated from the quadratic models, to rib level. To assess the significance of each parameter, a *t*-statistic was calculated by dividing the parameter estimate by its standard error. The *t*-statistic has a distribution with (*n-3*) degrees of freedom, where *n* is the sample size and 3 is the number of parameters estimated (*a, b*, and *c*) in the quadratic model. Given the value of the *t*-statistic and the number of degrees of freedom, the *P*-value was computed assuming a two-tailed test. A parameter was considered significantly different from 0 if the *P*-value was less than 0.05. The variable "Height" comprised 50 observations (Degrees of freedom = 47), while the variable "Rib thickness" included 49 observations (Degrees of freedom = 46). Intercostal muscle force was also related to vector stress using a nonlinear quadratic model.

Two-way ANOVA models with interaction were fitted to relate rib depth and rib height to both rib level and subject age. The models assessed the contributions of the two predictors to explaining variations in rib height and depth.

RESULTS

Rib Height and Thickness

Rib height increased with rib level, with a 13% increase between the 3rd and 7th levels, where the 7th/8th rib was the widest part or "equator" of the rib cage. This was statistically significant, $P < 0.001$ (*t*-test) (Fig. 3). Rib thickness showed a statistically significant 23% increase between the 3rd and 7th ribs, $P = 0.004$ (*t*-test).

Based on the general quadratic equation: $y = ax^2 + bx + c$, the model for predicted height at different levels between the 2nd and 12th ribs at the mid-axillary line is:

$$y = -0.0171x^2 + 0.2239x + 0.8306$$

where y is the predicted rib height and x is the rib level.

Similarly, the model for predicting thickness at different rib levels along the mid-axillary line between the 2nd and 12th ribs is:

$$y = -0.0084x^2 + 0.1125x + 0.3799$$

where y is the predicted rib thickness and x the is rib level.

The values of *a, b*, and *c* were all statistically significant for both height and thickness (each $P < 0.001$) (Fig. 6 and Table 2). The value of *c* corresponds to the *y*-intercept and the negative coefficient of x^2 implies a maximum turning point.

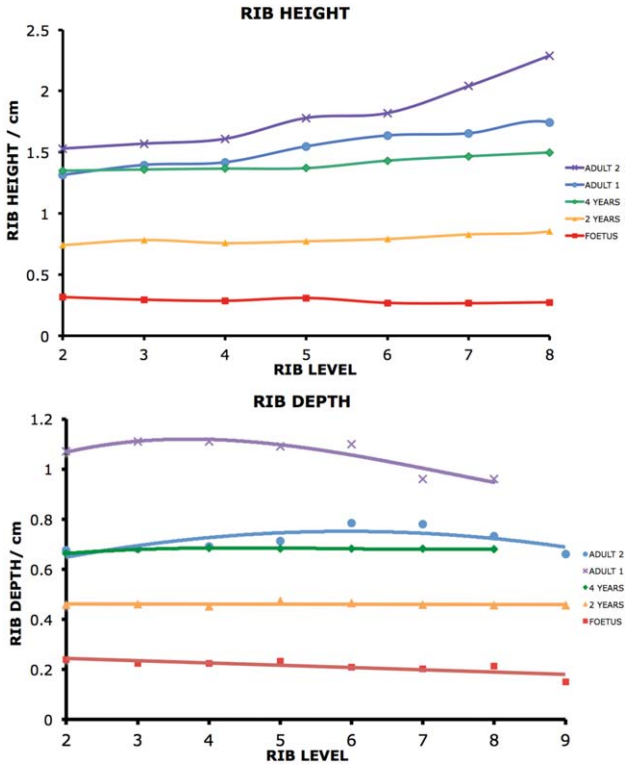

Fig. 5. Graphs displaying relationships between rib height and depth (thickness) with rib level for differently-aged individuals. Note that the ribs in the fetus are all identical, but intercostal muscle forces stretch rib height; and radial forces stress ribs with resultant increases in rib depth, with age acting as a significant predictor for both rib height and depth, $P < 0.001$ (2-way ANOVA). [Color figure can be viewed in the online issue, which is available at wileyonlinelibrary.com.]

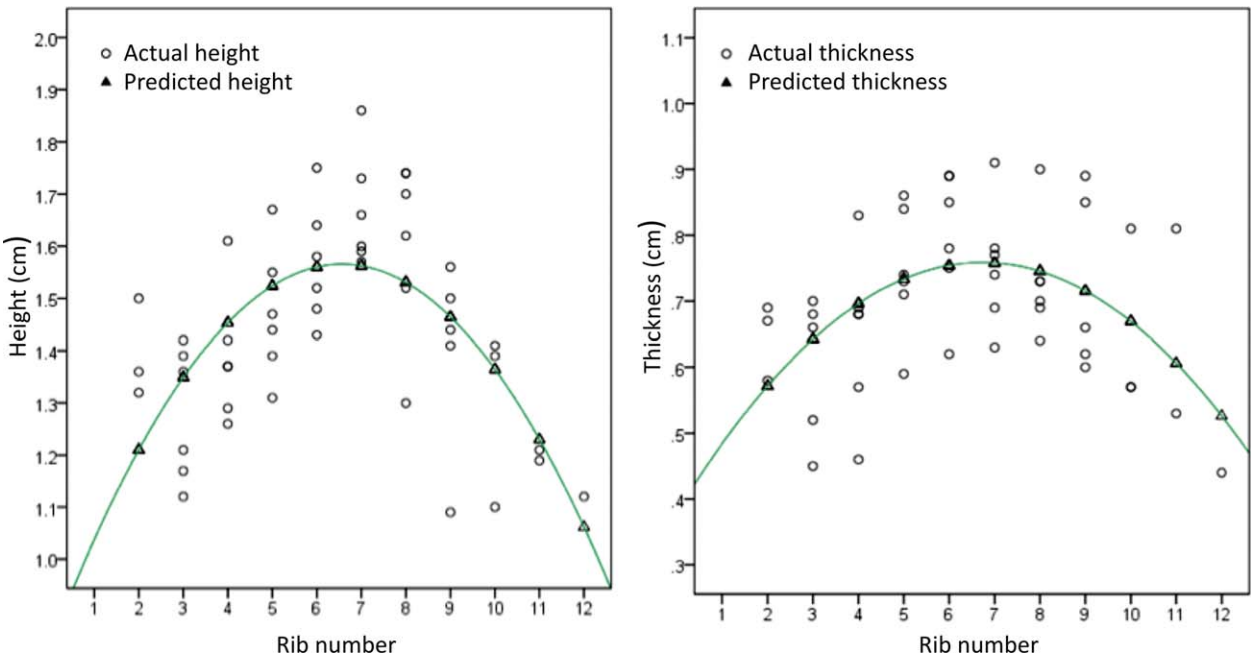

Fig. 6. Graph displaying quadratic relationships between rib thickness and rib height with rib level. The two quadratic models yield reasonably good fits; *R*-square = 0.412 for rib height model and *R*-square = 0.245 for rib thickness model. [Color figure can be viewed in the online issue, which is available at wileyonlinelibrary.com.]

For example, at the 5th rib level, when $x = 5$:

Predicted height, $y = -0.0171(5)^2 + 0.2239(5) + 0.8306 = 1.576$ cm

The maximum turning point occurs at: $x = -b/2a = -0.2239/2(-0.0171) = 6.49$ ribs i.e., between the 6th and 7th ribs. When $x = 6.49$, the predicted maximum height is 1.62 cm.

Rib Height and Intercostal Muscle Force

Intercostal muscle force was significantly related to vector stress (Fig. 4 and Table 1) (Pearson correlation $r = 0.944$, $P = 0.005$), but the relationship was not linear. Two contender nonlinear models were fitted: an exponential model, $y = e^{(ax+b)}$, and a quadratic model, $y = ax^2 + bx + c$. Both models provided better fits than the linear model (*R*-square = 0.891), but the fit of the quadratic model (*R*-square = 0.975) was considerably better than that of the exponential model (*R*-square = 0.912). Expected rib height, according to the quadratic model, followed the formula $y = ax^2 + bx + c$ where $a = 0.412$ (one-tailed Student's *t*-distribution, $P = 0.026$), $b = -3.699$ ($P = 0.033$), and $c = 3.267$ ($P = 0.029$) (Fig. 7):

Expected rib height = $0.412\ \text{Stress}^2 - 3.699\ \text{Stress} + 9.834$

The fetal ribs were of identical height and the rib cortices were all equal and featureless. There was a gradual increase in rib height with growth, especially during the first few years of life, the increase being proportional to chest diameter and accordingly more marked in the lower ribs, with the maximum occurring at the 7th or 8th rib, representing the "equator". With development/growth the difference in rib height becomes more evident.

Changes With Development

Rib depth. The two-way ANOVA with interaction model relating rib width to both rib level and age explained 95% of the total variance in rib width and

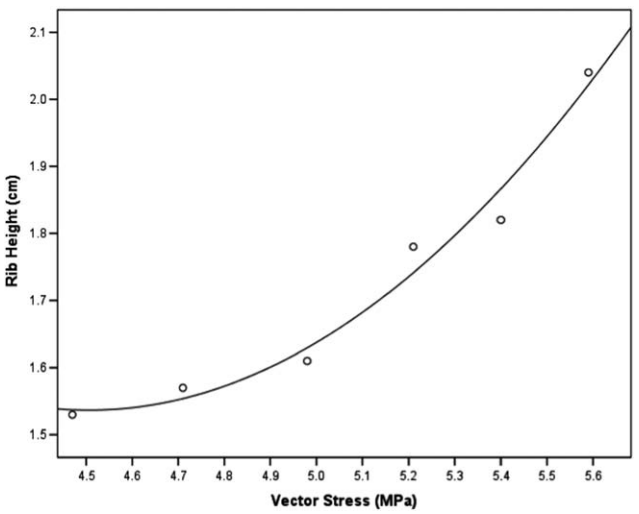

Fig. 7. Graph displaying quadratic relationship between rib height and vector stress (*R*-square = 0.975).

TABLE 1. Mean Values for Intercostal Muscle Vector Forces and Rib Height at Each Rib Level

Rib	Angulation/°	Circumferential§	Axial §	Vector stress §	Rib height/cm
2	35.2	2.15	1.49	4.45	1.53
3	34.5	2.33	1.54	4.69	1.57
4	35.2	2.46	1.59	4.96	1.61
5	36.1	2.56	1.63	5.19	1.78
6	37.2	2.63	1.65	5.38	1.82
7	39.0	2.67	1.66	5.57	2.04

Vector stress represents intercostal muscle force at 90° to rib. § $\times 10^6$Pa.

identified age as the sole significant predictor ($P < 0.0001$). Figure 5 reveals the increase in rib depth with age. The *P*-values of rib level ($P = 1.00$) and its interaction with age ($P = 0.963$) both exceeded the 0.05 criterion, indicating that they contributed insignificantly to explaining the variation in rib width. This is clearly revealed by the horizontal, almost parallel line graphs in Figure 5. As a general inference, rib width increases significantly with age irrespective of rib level.

Rib height. The two-way ANOVA with interaction model relating rib height to both rib level and age explained 94% of the total variation in rib height and again identified age as the sole significant predictor ($P = 0.0001$). Figure 5 reveals the increase in rib height with age. Rib level ($P = 0.957$) and the interaction between rib level and age ($P = 0.310$) were insignificant (*P*-values exceed 0.05), indicating that the line graphs were fairly horizontal and parallel.

DISCUSSION

Ribs are essential parts of the thorax (Kurihara, 1999), the rib cage being a feature of all vertebrates, but with different functions according to taxonomy. Tetrapods and fishes diverged during vertebrate evolution (Benton, 2005; Zimmer, 1999), a profound change well documented phylogenetically and from fossil discoveries (Shubin, 2008). Most tetrapods are quadrupeds, using four limbs for land locomotion, with the trunks suspended between the scapulae in the forelegs using the Serratus anterior muscles (Carrier, 2006). The thoracic ribs of quadrupeds are weight-bearing, transferring the load of the trunk to the forelimbs, and the thoracic ribs to which the Serratus attaches are stronger than normal ribs (Fujiwara, 2009). The function of the sternum in quadrupeds is to stabilize the ribcage by changing it from an incomplete ring to a stable complete one (Carrier, 2006).

Human ribs are not weight-bearing owing to the bipedal stance, which also results in the vertebral column moving ventrally to aid the center of balance. This migration of the spine occurs in infancy in both humans and apes; in the fetus, the transverse and sagittal thoracic diameters are equal (Openshaw, 1984) and the spine lies at the back of the thorax as it does in monkeys and quadrupeds (Schultz, 1956), the scapula migrating backwards on the rib cage at the same time (Schultz, 1961).

The external dimensions of ribs vary such that their height and width are maximal at the widest part of the ellipsoid human chest and taper towards the lower ribs and the third rib. The height of the ribs was significantly associated with the intercostal muscle force, calculated as the wall tension in a pressure vessel model simulating the chest during coughing. In the brief episode of equilibrium during coughing, the pressure vessel wall tension must equal the resultant vector of the tension within the intercostal muscles. As pressure vessel wall tension varies with location within the vessel, with forces approximately proportional to the radius of curvature, different ribs are exposed to forces that differ with rib level. They respond to these forces by stretching along their direction to increase both their height and thickness (Fig. 5).

TABLE 2. Parameter Estimates for *a, b*, and *c;* 95% Confidence Intervals, Standard Errors, *P*-Values, and *R*-Square Values for Each Nonlinear Quadratic Models

Parameter estimates	*R*-square	Parameter	Estimate	Standard error	*P*-value	95% Confidence interval	
						Lower bound	Upper bound
Ribheight with rib level	0.412	*a*	−0.0171	0.0030	< 0.001	−0.0230	−0.0111
		b	0.2239	0.0396	< 0.001	0.1443	0.3036
		c	0.8306	0.1194	< 0.001	0.5904	1.0708
		Expected rib height = −0.0171 (Rib level)^2 + 0.2239 (Rib level) + 0.8306					
Rib thickness with rib level	0.245	*a*	−0.0084	0.0022	< 0.001	−0.0128	−0.0040
		b	0.1125	0.0292	< 0.001	0.0537	0.1713
		c	0.3799	0.0889	< 0.001	0.2010	0.5589
		Expected rib height = −0.0084 (Rib level)^2 + 0.1125 (Rib level) + 0.3799					
Rib height with vector stress	0.975	*a*	0.412	0.131	0.026	−0.004	0.828
		b	−3.699	1.310	0.033	−7.869	0.471
		c	9.834	3.267	0.029	−0.562	20.230
		Expected rib height = 0.412 Stress^2 − 3.699 Stress + 9.834					

All the muscles involved in respiration, including the direct and indirect respiratory muscles, can affect the ribs. The act of coughing uses the abdominal muscles balanced against the back muscles to generate high intra-thoracic pressures. The basic action of the muscles involved in respiration and coughing is to produce cyclical changes in intra-thoracic pressure that effectively turn the thorax into a pressure vessel. Although in principle the effect of coughing could be modeled by vector forces acting in three dimensions representing the action of every muscle on the skeleton involved directly or indirectly in ventilation and coughing, in practice the magnitude and direction of these muscle actions would be difficult to model accurately, especially the indirect effects of the back and abdominal muscles on the chest cage. Another approach is to consider that the chest meets the criteria for a thin-walled pressure vessel (Pai, 2005; Casha, 2012), with a diameter more than twenty times its wall thickness. The sum of the forces acting on the chest wall during breathing or coughing must obey the Law of Laplace, which determines wall tension in a vessel with a distending pressure. The pressure differences during respiration are modest, but the pressure during maximal coughing can reach levels as high as 40 kPa (Murray and Nadal, 1994; Lumb, 2000; Talbert, 2005), aided by a rapid rise in intra-abdominal pressure (Aspden, 1992).

Laplace's law indicates that different ribs are under different levels of tension or force during coughing. The upper part of the chest wall has the least stress simply because the chest diameter is smallest there. The angles of the ribs have the highest stress since their radius of curvature is smallest. By determining the stresses on the ribs, the magnitude of the stimulus for adaptation of the ribs could be calculated. This impetus for bone adaptation starts after birth and continues during childhood and adult life. Intercostal muscle force was a statistically significant determinant of rib height, with the statistical model explaining 97.5% of the possible effect.

The radial stresses in thin-walled pressure vessels are an order of magnitude lower than the tangential membrane stresses (Young and Budynas, 2002) and can usually be disregarded, so the wall stresses can be assumed to be uniform across the internal and external surfaces (Timoshenko, 1942). This means that the effects of axial forces on rib height are much greater (10×) than those of the radial forces on rib thickness, so the round fetal ribs are stretched into their adult shape. As with all pressure vessels, the magnitude of the radial forces is proportional to the tangential radius of curvature, meaning that apical forces are lower than forces at the "equator" of the rib cage, resulting in thicker ribs at the 6th and 7th spaces, becoming narrower towards the apex.

This article has shown how rib morphology is influenced by environmental factors, displaying the behavior of bone when exposed to continuous forces. However, additional work is required for a better understanding of this mechanism, and it is hoped that this study will stimulate further investigations in the field. This understanding of the variation of stresses in the chest wall could be important in chest wall reconstruction and also in predicting rib fractures, which is useful for crash test-dummy development.

CONCLUSIONS

The external morphology of ribs, in particular their height and thickness, can be predicted by an ellipsoid pressure vessel model of the chest, suggesting that external environmental pressures are important in determining human rib morphology.

ACKNOWLEDGMENTS

The authors declare no conflict of interest and would like to express their gratitude to the cadaver donors and their families who participated in the medical school cadaveric donation program and to Mr. Peter Bentley-Brown for assistance with specimen preparation.

REFERENCES

Aspden RM. 1992. Review of the functional anatomy of the spinal ligaments and the lumbar erector spinae muscles. Clin Anatomy 5:372–387.

Astley HC, Jayne BC. 2007. Effects of perch diameter and incline on the kinematics, performance and modes of arboreal locomotion of corn snakes (Elapheguttata). J ExpBiol 210:3862–3872.

Beck TJ, Oreskovic TL, Stone KL, Ruff CB, Ensrud K, Nevitt MC, Genant HK, Cummings SR. 2001. Structural adaptation to changing skeletal load in the progression toward hip fragility: The study of osteoporotic fractures. J Bone Miner Res 16:1108–1119.

Benton MJ. 2005. Vertebrate Palaeontology. 3rd ed. Oxford: Blackwell Publishing.

Britz R, Bartsch P. 2003. The myth of dorsal ribs in gnathostome vertebrates. ProcBiolSci 270 Suppl 1:S1–S4.

Carrier DR, Deban SM, Fischbein T. 2006. Locomotor function of the pectoral girdle 'muscular sling' in trotting dogs. J ExpBiol 209: 2224–2237.

Casha AR, Manche A, Gatt R, Duca E, Gauci M, Schembri-Wismayer P, Camilleri-Podesta MT, Grima JN. 2014. Mechanism of sternotomy dehiscence. Interact Cardiovasc Thorac Surg 19:617–621.

Casha AR, Manche A, Gauci M, Camilleri-Podesta MT, Schembri-Wismayer P, Sant Z, Gatt R, Grima JN. 2012. Placement of transsternal wires according to an ellipsoid pressure vessel model of sternal forces. Interact Cardiovasc Thorac Surg 14:283–287.

Chen EJ, Novakofski J, Jenkins WK, O'Brien WD, Jr. 1996. Young's modulus measurements of soft tissues with application to elasticity imaging. Ultrasonics Ferroelectrics Frequency Control IEEE Transactions 43:191–194.

Frost HM. 2003. Bone's mechanostat: A 2003 update. Anat Rec A Discov Mol Cell Evol Biol 275:1081–1101.

Grivas TB, Burwell RG, Purdue M, Webb JK, Moulton A. 1992. Segmental patterns of rib-vertebra angles in chest radiographs of children: Changes related to rib level, age, sex, side and significance for scoliosis. Clin Anat 5:272–288.

Halliday D. 1997. Pascal's Principle, Fluids. In: Halliday DRR, Walker J, editors. Fundamentals of Physics. New York: Wiley. p 355–356.

Kurihara Y, Yakushiji YK, Matsumoto J, Ishikawa T, Hirata K. 1999. The ribs: Anatomic and radiologic considerations. Radiographics 19:105–119; quiz 151–102.

Li Z, Kindig MW, Subit D, Kent RW. 2010. Influence of mesh density, cortical thickness and material properties on human rib fracture prediction. Med Eng Phys 32:998–1008.

Lumb AB. 2000. Nunn's Applied Respiratory Physiology. Oxford: Heinemann.
Murray JFNJA. 1994. Textbook of Respiratory Physiology. Philadelphia: WB Saunders and Company.
Openshaw P, Edwards S, Helms P. 1984. Changes in rib cage geometry during childhood. Thorax 39:624–627.
Pai S, Gunja NJ, Dupak EL, McMahon NL, Roth TP, Lalikos JF, Dunn RM, Francalancia N, Pins GD, Billiar KL. 2005. In vitro comparison of wire and plate fixation for midline sternotomies. Ann ThoracSurg 80:962–968.
Papadakis S. 1977. Design of Pressure Vessels. Masters thesis. Montreal, Canada: Concordia University. p 105.
Pender DJ. 2009. A model analysis of static stress in the vestibular membranes. TheorBiol Med Model 6:19.
Pezowicz C, Glowacki M. 2012. The mechanical properties of human ribs in young adult. Acta Bioeng Biomech 14:53–60.
Schultz AH. 1956. Postembryonic age changes. Primatologia 1:887–964.
Schultz AH. 1961. Vertebral column and thorax. Primatologia 4:1–66.
Shubin N. 2008. Your Inner Fish: A Journey into the 3.5-Billion-Year History of the Human Body. 1st Ed. New York: Pantheon Books.
Talbert DG. 2005. Paroxysmal cough injury, vascular rupture and 'shaken baby syndrome'. Med Hypotheses 64:8–13.
Young WC, Budynas RG. 2002. Roark's Formulas for Stress and Strain. 7th ed. New York: McGraw-Hill.
Zimmer C. 1999. At the Water's Edge: Fish with Fingers, Whales with Legs, and How Life Came Ashore but Then Went Back to Sea New York: Simon & Schuster.